

Propagation of Disturbances in AC Electricity Grids

Samyak Tamrakar^{a,b}, Michael Conrath^a, Stefan Kettemann^{a,c}

^aJacobs University, Department of Physics and Earth Sciences, Campus Ring 1, 28759 Bremen, Germany

^bInstitute of Physics, Carl von Ossietzky Universität Oldenburg, Ammerländer Heerstraße 114-118, 26129 Oldenburg

^cDivision of Advanced Materials Science, Pohang University of Science and Technology (POSTECH), San 31, Hyoja-dong, Nam-gu, Pohang 790-784, South Korea

Abstract

The energy transition towards high shares of renewable energy resources will affect the dynamics and the stability of electricity grids in many ways. It is therefore crucial to understand its impact. We aim to contribute to this understanding by solving the dynamic swing equations describing the coupled rotating masses of synchronous generators and motors. On different grid topologies we identify parameter regimes with very different transient dynamics: the disturbance may either decay exponentially in time, superimposed by oscillations, with the fast decay rate of a single node, or with a smaller decay rate without oscillations. Most remarkably, as the inertia is lowered, the nodes may become more correlated, slowing down the spreading of a disturbance, decaying slowly with a power law in time. We show that this collective effect exists in meshed transmission grids, but is absent in tree grids. We conclude by discussing consequences for the stability of transmission grids if no measures are undertaken to substitute the inertia of conventional power plants.

In order to cover the increasing human energy demand by renewable energy resources and to ensure that this energy will be available wherever and whenever it is needed, more efficient energy transport and storage technologies need to be developed. The fluctuations in generated power by wind turbines and solar cells - both in time and geographically - demand to explore new strategies to store energy on all time scales and to distribute the power in the grid smartly. At the same time, the spreading of critical disturbances throughout the grid has to be prevented to ensure the stability of the entire grid. Renewable energy resources fluctuate strongly in time on time scales as small as seconds. Moreover the inverter-connected wind turbines and solar cells provide no inertia [1]. This is in contrast to conventional generators, whose rotating masses hold inertia and thereby momentary power reserve available for the grid, which makes the grid resilient and prevents strong fluctuations of the grid frequency on time scales of several seconds [2, 3]. As the inertia in the grid keeps decreasing with higher share of renewables,

the grid is responding on shorter time scales to disturbances. It is therefore essential to understand the impact of this development on the stability of electricity grids. In this article, we aim to find out if and how the propagation of disturbances in AC grids is modified when the grid inertia from the rotating masses of generators is decreasing.

The dynamic interaction and response of generators and consumers is studied modeling the grid as a network of nonlinear oscillators [2, 3, 4, 5, 6, 7]. These nonlinear swing equations describe the dynamics of coupled rotating masses by a system of coupled differential equations for local rotor angles φ_i , where i denote the grid nodes. As we aim to contribute to the understanding of how disturbances evolve with time in AC grids, we consider control free grids without primary and secondary control measures [1, 2, 3]. The origin of disturbances can be fluctuations in generating power or sudden changes of transmission line capacitance. We solve the nonlinear dynamic power balance equations numerically and explore how a local perturbation propagates with time throughout the

grid. We analyze these numerical results, employing analytical results as obtained from mapping the swing equations on discrete linear wave equations for small perturbations [8]. Depending on the geographical distribution of power, grid power transmission capacity and topology we find that the disturbance may either decay exponentially in time with the decay rate of a single oscillator Γ^0 , or exponentially with a smaller decay rate $\Gamma < \Gamma^0$, or, even more slowly, decaying with a power law in time. Such a slow power law decay arise together with a slow, diffusive propagation [8].

Results

Grid Topologies. Aiming at a systematic approach, we consider three different grid topologies. Firstly, the Cayley tree grid, Fig. 1 a), resembles typical distribution grids which are preferably operated in such a tree-like fashion to pinpoint and repair failures more easily. Starting from a center, a constant number of branches grows outward in a given number of branching levels, each time with the same branching number b . Hence, the tree grids are characterized by b and the level l of branching, the distance between neighbored nodes a and the total number of nodes N . An important characteristic of grids is the degree d_i , the number of links connecting node i to any other node. The degree of this tree grid is $d = b + 1$, with the exception of the edge nodes, which have degree $d = 1$. Secondly, the square grid, Fig. 1 b). It is a simple meshed topology, used as basic model for transmission grids with their strict redundancy demand to guarantee continuing operation even when a single line fails (n-1 criterion). These square grids are characterized by the distance between neighbored nodes a , the linear grid size L and the number of nodes $N = (L/a)^2$. Their degree is constant, $d = 4$, except at edges ($d = 3$) and corners ($d = 2$). Thirdly, we choose the German transmission grid, Fig. 1 c) as a real-world example with an irregular realistic topology, which is inhomogeneous and highly meshed. As reference for the German transmission grid, the open-source SciGRID dataset was used [9]. Excluding island nodes in it, the largest connected network of the four highest voltage levels, 400 kV, 380 kV, 220 kV as well as some 110

kV lines, was adopted as grid model. It comprises $N = 502$ nodes and 673 links. It has a wide distribution of degree d_i , Fig. 2, with average degree $\langle d_i \rangle = 2.7$ and typical degree $d_{typ} = \sqrt{\langle d_i^2 \rangle} = 4.1$. Excluding stubs, singly connected nodes, mostly due to the artifact that this data set does not include the transnational European grid, we get an average degree $\langle d_i \rangle = 3.5$.

Dynamic AC Grid Model. 3-phasic alternating current (AC) electric grids can be modeled by active power balance equations [4, 5, 6, 10, 11, 12]. Since the three phases are typically loaded and operated symmetrically, they can effectively be reduced to a single phase. Furthermore, linking the grid nodes, purely inductive lines are assumed, neglecting the Ohmic losses along the lines, which are relatively small in high voltage transmission grids. The combined inductance of an individual 3-phasic line between nodes i and j is L_{ij} . The line power capacity is then $K_{ij} = |V_i||V_j|/(\omega L_{ij})$ where V_i, V_j are the voltages at node i and j . ω is related to the grid frequency $f = 50$ Hz by $\omega = 2\pi f$. We will focus on the dynamics of the phases φ_i , while the voltage amplitudes are taken constant, since they typically change only on larger time scales. We assume the same voltage amplitude throughout the grid, so that $V_i = V \exp(i\phi_i)$ with ϕ_i being the voltage phase. Since our main goal is to study the influence of the grid topology and the inertia on the phase dynamics we assumed that all links have equal inductance L and thus equal power capacity $K = V^2/(\omega L)$. Thus, the power capacity linking nodes i and j is given by $K_{ij} = K A_{ij}$, where A_{ij} is the adjacency matrix of the grid. Under these conditions, the stationary active power flow in the grid is obtained from Kirchhoff's laws as function of the voltage phases ϕ_i as

$$P_i = K \sum_j A_{ij} \sin(\phi_i - \phi_j) , \quad \sum_i P_i = 0, \quad (1)$$

with the second equation being the power balance condition, which has to be preserved at any time in order to avoid frequency shifts and is therefore controlled by grid operators. However, the nodal phases vary with time. The constant grid frequency gives a phase shift which increases linearly in time as ωt , independently of the node i . Denoting the solution of the stationary balance equation Eq. (1) by the phase

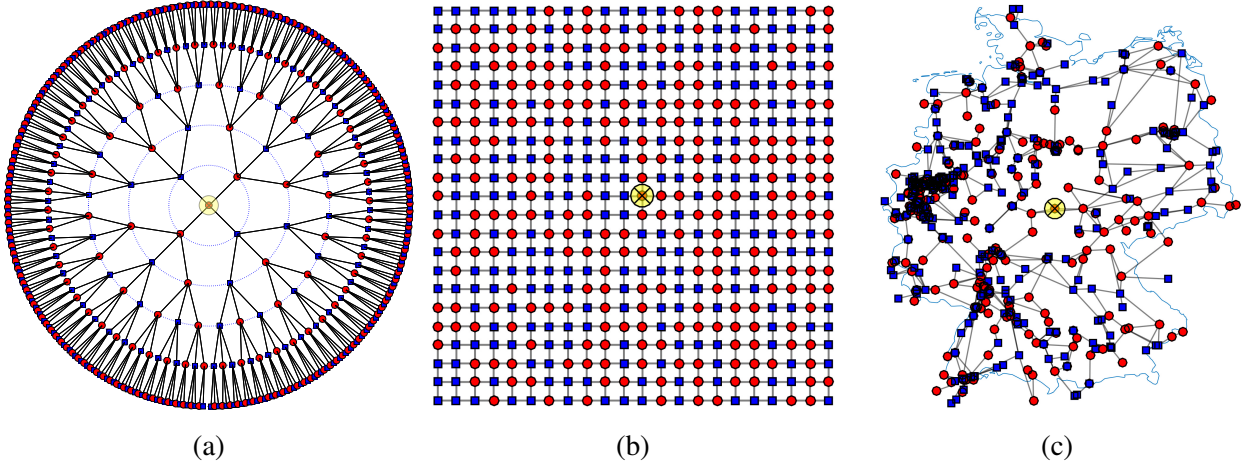


Figure 1: Grid topologies under consideration in the present study. (a) Cayley tree grid with 5 branching generations and 3 new branches ‘growing’ from every point giving $N = 484$ nodes and 483 links. (b) 22×22 square grid with $N = 484$ nodes, 924 links and random arrangement of generators and consumers. (c) German transmission grid model with $N = 502$ nodes and 673 links [9]. The parameters of square and tree grid, respectively, have been chosen in favor of comparable size to the German grid. Red circles represent generators, blue squares represent motors and the yellow circle with ‘X’ marks the spot where a perturbation is applied.

shift θ_i^0 , we can write

$$\phi_i(t) = \omega t + \theta_i^0 + \alpha_i(t) , \quad (2)$$

with the additional dynamic, time dependent phase shift denoted by $\alpha_i(t)$. In the present work all grid nodes are assumed to be connected to rotating machines, either synchronous generators or motors with inertia J_i . All rotating machines and therefore all nodes are assigned an equal magnitude of electric power P , which is either positive (generator) or negative (motor). Consequently, $P_i = s_i P$, with $s_i \in \{+, -\}$ and $J_i = J$. The phase dynamics is then governed by the balance of the change in kinetic energy, the energy dissipation in the machines, and the electrical energy exchange with adjacent grid nodes, yielding the swing equations [4, 5, 6].

$$P_i = \left(\frac{J}{2} \frac{d}{dt} + \gamma \right) \left(\frac{d\phi_i}{dt} \right)^2 + \sum_j F_{ij}, \quad (3)$$

where γ is the damping constant and $F_{ij} = K_{ij} \sin(\phi_i - \phi_j)$ is the power flow in the transmission line between nodes i and j . We note that, if the nodes would not be coupled by the transmission lines, the phase at each node would decay exponentially fast with the local relaxation time $\tau = J/\gamma$, increasing with inertia J and decreasing with damping parameter γ . Therefore, when studying the effect of the coupling between the nodes, it is convenient to scale the time with relaxation time τ . In order

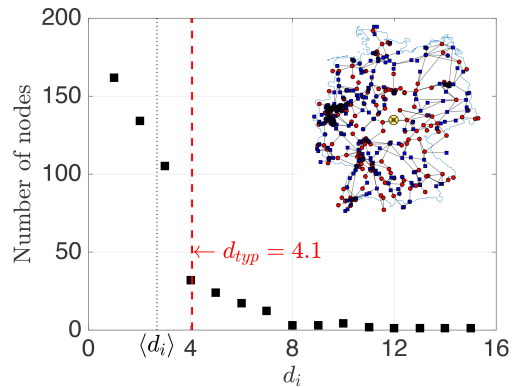


Figure 2: Distribution of node degree d_i for German transmission grid.

to study the spreading of perturbations, the temporal and spatial dependence of α_i , we insert Eq. (2) into Eq. (3) and for small phase velocities, $\partial_t \alpha_i \ll \omega$, we arrive at the swing equations in dimensionless form,

$$\tau^2 \partial_t^2 \alpha_i + 2\tau \partial_t \alpha_i = s_i \Pi_P - \Pi_K \sum_j A_{ij} \times \sin(\theta_i^0 - \theta_j^0 + \alpha_i - \alpha_j), \quad (4)$$

with dimensionless parameters $\Pi_P = JP/(\gamma^2 \omega)$ and $\Pi_K = JK/(\gamma^2 \omega)$.

Transient Dynamics. Now, we proceed to solve the nonlinear swing equations Eq. (4) on the different grid topologies shown in Fig. 1 for a set of parameters (τ, Π_K, Π_P) , in order to study the transient

behavior of the AC grid when it is perturbed by a local disturbance. As disturbance of the stationary

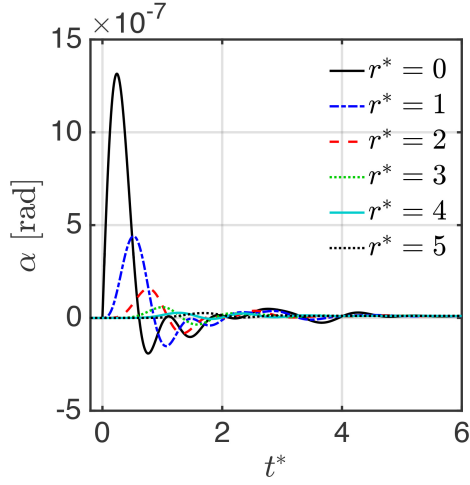


Figure 3: Phase perturbation $\alpha(r^* = r/a, t^* = t/\tau)$ for the $b = 3$ Cayley tree grid at nodes on different distances $r = la$ away from the center node.

state we increase the power for a short time interval $0 \leq t \leq \Delta t_{pert}$, at the grid node marked with ‘x’ in the different grid topologies, Fig. 1. We choose it as one per mille of the initial power P , corresponding to a perturbation energy $E_{pert}^0 = 0.001\Pi_P \cdot \Delta t_{pert}$. The resulting transient behavior of the phase deviation $\alpha(t)$ is shown exemplary in Fig. 3 for the Cayley tree grid of Fig. 1 a) as function of rescaled time $t^* = t/\tau$ for the parameters ($\Pi_K = 10, \sigma = \Pi_P/\Pi_K = 0.08$). We see that the phase at the disturbed node, $r^* = 0$ (The distance between any two nodes r_{ij} is defined as the number of edges in a shortest path connecting them [13]; $r^* = r/a$.) is perturbed first, reaching a maximum after a delay time, and then decaying in an oscillatory manner. As expected, phases of nodes further away from the origin of the disturbance are perturbed later and reach smaller amplitudes. We will analyze this temporal and spatial behavior quantitatively in the following.

Another way to visualize this transient behavior is the phase portrait shown exemplary in Fig. 4, a plot of phase velocity $\dot{\alpha}_i$ versus phase α_i . We see in the upper figure that the disturbance remains within the basin of attraction of the attractive fixed point for $\Pi_K = 100$ and σ not exceeding 0.2. There is a slight shift of the phase to which the perturbation decays at the end, which we find to be due to a global phase

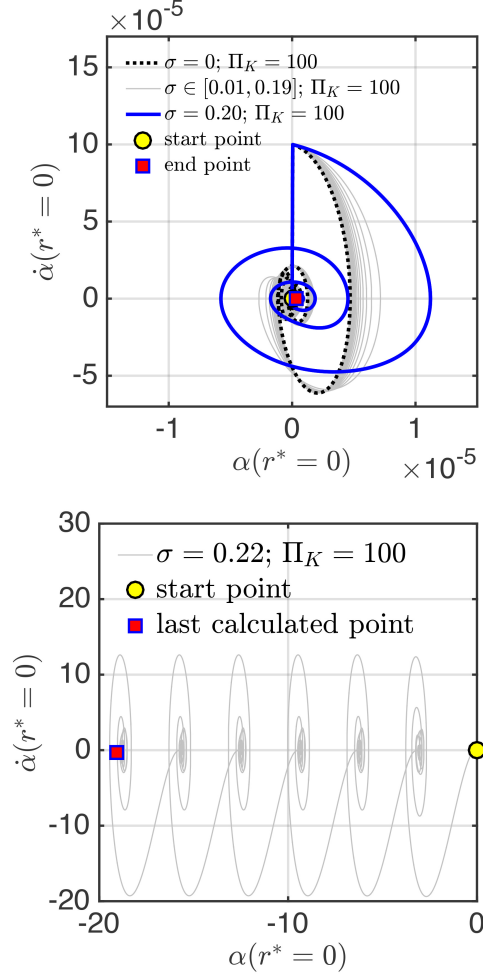


Figure 4: Phase portrait $\dot{\alpha}(r, t^*)$ versus $\alpha(r, t^*)$ for the $b = 3$ Cayley tree grid for $\Pi_K = 100$ and various σ .

shift of all nodes induced by the disturbance at the center node. In the lower figure it is seen that the perturbation destabilizes the grid when $\sigma = 0.22$, where the phase deviation increases unboundedly. Since we are interested in the propagation of small disturbances which do not destabilize the system, we review next the conditions for stability in order to choose the size of the disturbance accordingly.

Stability. Not all values of the parameters Π_P and Π_K allow for a stable stationary state. Without any disturbance, the criterion to distinguish between stable (allowed) and unstable (forbidden) parameters is the existence of a non-complex solution for the stationary state, Eq. (1). Thus, the ratio $\sigma = \Pi_P/\Pi_K$ determines whether parameters are allowed or forbidden and a critical value σ_c exists depending on grid topology and power distribution. If the power distribution is $P_i = s_i P$, with $s_i \in \{+, -\}$, and there

are no clusters of consumers or clusters of generators, the critical value at node i is given by $\sigma_{ci} = d_i$, where d_i is the node degree. Thus, the critical value below which all nodes of the whole grid are stable is given by $\sigma_c = \min(d_i)$. For a general distribution of P_i , there can be clusters of generators or consumers. Then, the critical value σ_c is determined by the size and form of the clusters. If a cluster of generators has the total power $P_C = \sum_{\text{cluster}} P_i$, with an effective degree d_C , as obtained by counting the number of consumers which are directly coupled to that cluster, the critical value of $\sigma = \Pi_{P_i}/\Pi_K$ above which no stable solution exists, is given by $\sigma_c = \min(P d_C/P_C)$.

Depending on the magnitude of the disturbance it can destabilize the grid already at $\sigma < \sigma_c$. In the Suppl. I. we derive a typical upper limit for the size of the perturbation α before it kicks the system out of the stable region. We find that the disturbance can destabilize the grid at smaller values $\sigma^*(\alpha) < \sigma_c$. $\sigma^*(\alpha)$ coincides with σ_c only in the limit, when the perturbation amplitude is vanishing, $\sigma^*(\alpha \rightarrow 0) = \sigma_c$.

Classification of Transient Dynamics: Parametric Phase Diagrams. Next, in order to analyze the transient behavior of disturbances we calculate the absolute values of the changes in power flow in the transmission line between nodes i and j , $\Delta F_{ij}(r) = |F_{ij}(r) - F_{ij}^0(r)|$, averaged over all transmission lines at a distance r from the disturbance and divided by its maximum value,

$$\Delta f(r^*, t^*) = \frac{\langle \Delta F_{kl}(r^*, t^*) \rangle}{\max_t (\langle \Delta F_{kl}(r^*, t^*) \rangle)}. \quad (5)$$

In Figs. 5 we show examples for transient dynamics $\Delta f(r^*, t^*)$ in three grid topologies for several different parameter values Π_K, σ . If there is no stable solution the phase perturbation increases without bound as seen in the example of Fig. 5 c) for the Cayley tree grid and in the lower phase portrait of Fig. 4. In order to find the parametric dependence systematically, we varied both parameters Π_K and σ in small steps. By mapping all parameters for which we find unstable solutions, we find unstable parameter regions for $\sigma > \sigma_c$, as shown in red in Fig. 6 a) for the tree grid, in Fig. 6 b) for the square grid with periodic arrangement, in Fig. 6 c) for the square grid with random arrangement of consumers and generators, and in Fig. 6 d) for the German transmission grid.

The critical values of σ_c depend on the grid topologies: For the Cayley tree grid with $b = 3$ we find $\sigma_c = 0.2$, for the square grid with periodic arrangement $\sigma_c = 2.00$, for the Square grid with random arrangement $\sigma_c = 1.25$ and for the German transmission grid $\sigma_c = 0.33$. In the stable regions we identify the following three qualitatively different transient behaviours:

The perturbation decays *exponentially fast* (FE) with local relaxation rate Γ_0 superimposed by oscillations, as seen in exemplary transients at the origin of the disturbance $\Delta f(0, t^*)$ in Fig. 5 a) for tree grid, in Fig. 5 f) for periodic square grid, in Fig. 5 i) for random square grid and in Fig. 5 l) for German transmission grid. All parameter sets showing FE behavior are plotted in Fig. 6 a)-d) as green circles.

We observe the decay to be exponential with a smaller relaxation rate $\Gamma < \Gamma_0$, for a large interval of time $t - t_0 \gg \tau$ as seen in Figs. 5 b) for the tree grid, e) and h) for the square grids and k) for the German grid. The corresponding parameter sets which show such *slow exponential relaxation* (SE) are shown in Fig. 6 a)-d) as yellow squares.

In the green shaded area fast relaxation (FE) is expected to occur according to analytical results of the next section, limited by the dashed lines in Fig. 6 a)-c), a plot of Eq. (12) for the tree grid and of Eq. (8) for the square grids, respectively. For the German grid, we indicate the boundary of that region in Fig. 6 d) by a dotted line, as suggested by numerical results. The yellow shaded areas in Fig. 6 a)-c) show where slow relaxation (SE) is expected to occur according to the analytical results. There is good agreement, the slight inconsistency is in a region where we observe deviations of Γ from Γ_0 by only a few percent, well within the estimated errorbars of the numerical results. This parametric dependence of the relaxation rate is also seen in Fig. 7 for the $b = 3$ Cayley tree grid where we plot the decay rate $\Gamma(\sigma)$ in units of local relaxation rate Γ_0 , as obtained by fitting the transient behavior with an exponential decay.

Finally, and most surprisingly, we observe an even slower decay with a *power law* in time in square grids and in the German grid, as seen in exemplary plots Figs. 5 d) and g) for the square grids and j) for the German grid. The power is close to 2, in good agreement with diffusive behavior for $\Delta f(t)$, as obtained

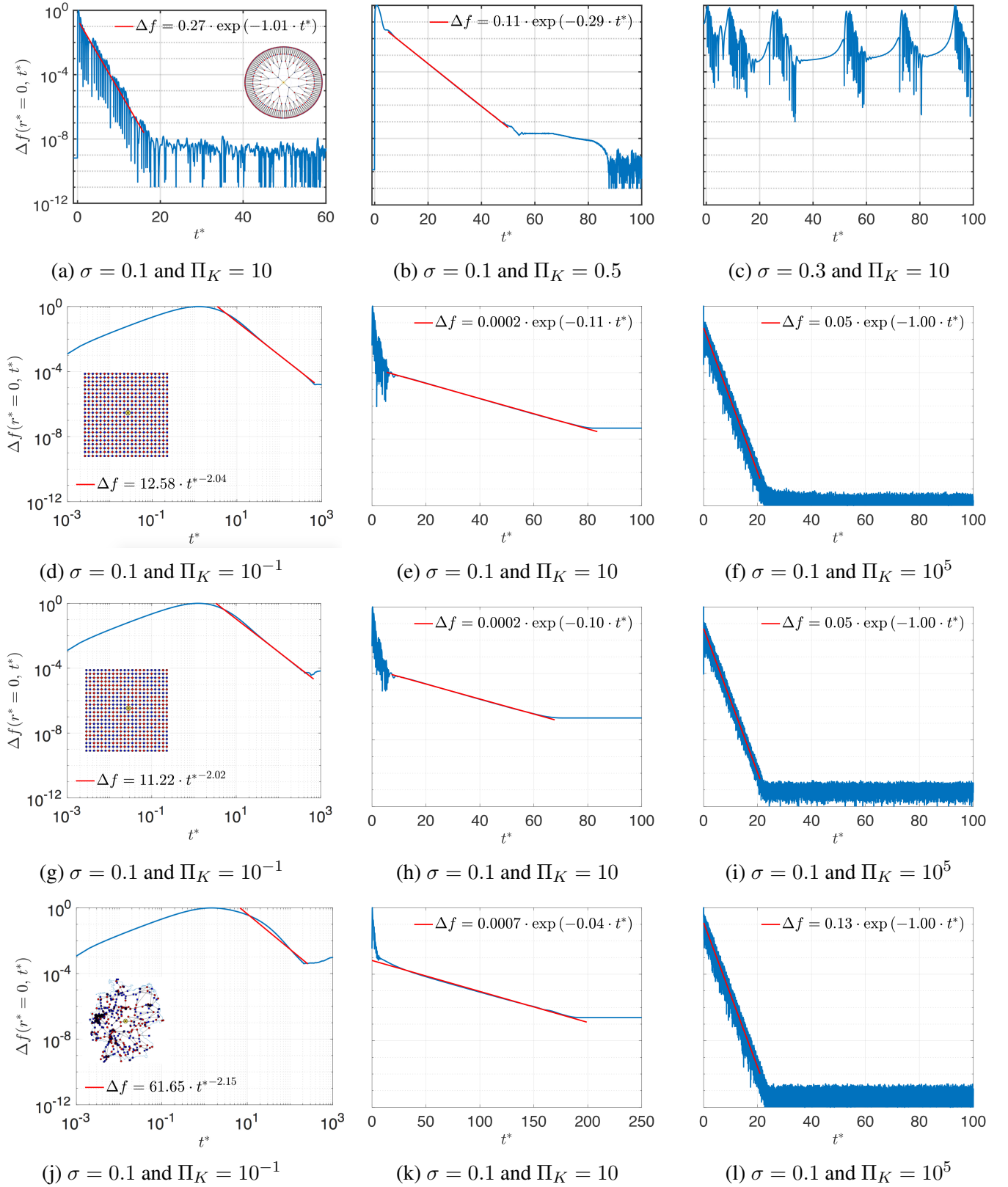


Figure 5: Averaged change of power flow as function of time (Blue Curves) at $r^* = 0$ with disturbance in power $\delta P = 0.001P$ for (a)-(c) a Cayley tree grid ($N = 484$) for three exemplary sets of parameters, (d)-(f) a square grid, $L = 22$, with periodic arrangement, (g)-(i) a square grid, $L = 22$, with random arrangement, (j)-(l) German transmission grid with random arrangement of generators and motors. Each for three exemplary sets of parameters correspond to three distinct stability regions. We fitted the numerical results (blue) with exponential and power law functions (red).

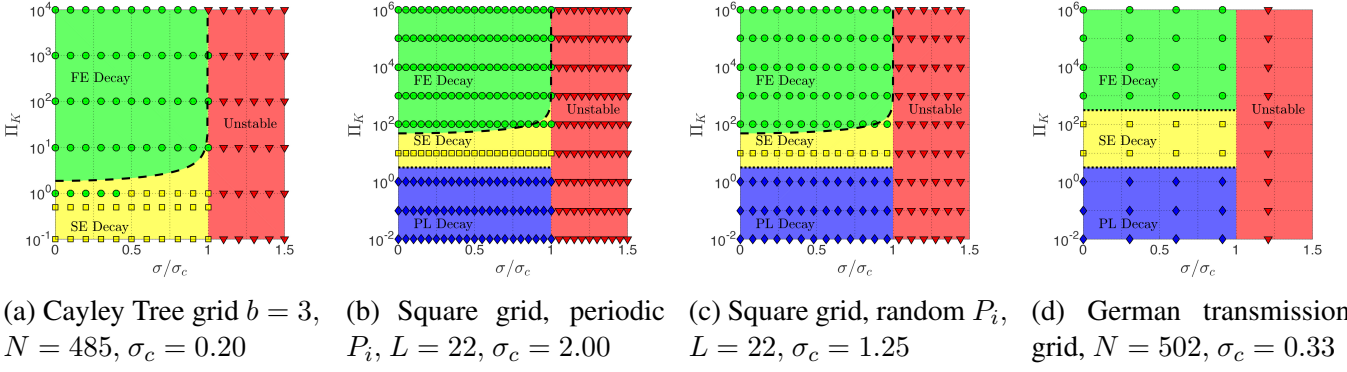


Figure 6: Phase diagrams as function of parameters Π_K and σ . Red triangle, green circle, yellow square and blue diamond represent numerically verified parameters that make the grid unstable, that result in fast exponential (FE) decay, in slow exponential (SE) decay and in power law (PL) decay, respectively. Red, green and yellow shaded regions represent parameters that, according to analytical results, are unstable, to have FE decay and SE decay, respectively. Blue shading represents the numerically obtained region with PL decay. In Fig. (a) dashed black line is the phase boundary between FE and SE decay according to Eq. (12), in Figs. (b) and (c) dashed black lines, Eq. (8). For Figs. (b), (c) and (d), dotted black lines are numerically obtained boundaries.

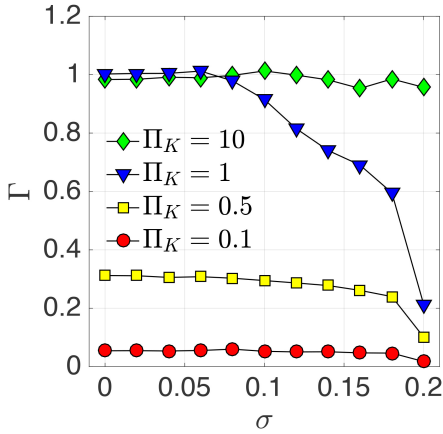


Figure 7: The decay rate $\Gamma(\sigma)$ in units of local relaxation rate Γ_0 in the $b = 3$ Cayley tree grid for different values of Π_K , as obtained by fitting transient behavior with exponential decay.

for a model square grid by an analytical derivation [8], see the next section, Eq. (17). Although that result was derived for square grids only, the numerical results indicate that such diffusive behavior may occur also in other meshed grids, as the example of the German grid shows at small values of the parameter $\Pi_K < 2$, Fig. 5 j). Thus, although the local relaxation time $\tau = J/\gamma$ decreases when the inertia J is lowered, more nodes become correlated and thereby the spreading of a disturbance is slowed down to a collective diffusive spreading for times $t > \tau$ as Π_K and thereby the inertia J is lowered.

Diffusive propagation results also in a slowed spa-

tial spreading of disturbances, as seen by calculating the expectation value of the squared distance, $\langle r_t^2 \rangle = \sum_i \alpha_i^2(t) (r_i - r_j)^2 / \sum_i \alpha_i^2(t)$. Diffusion results in linear increase with time for times $t - t_0 > \tau$, while ballistic motion gives a faster, quadratic increase. In Fig. 8 b) the result is shown for a square grid with periodic arrangement of P_i . We find that $\langle r_t^2 \rangle$ increases initially very fast for times $t - t_0 < \tau$.

For small $\Pi_K = 0.1$ it slows down to a power law increase for $t - t_0 > \tau$ with $\langle r_t^2 \rangle \sim t^\beta$, where $\beta = 1.12$ fits the data, which is a very strong indication of diffusive propagation in square grids with small inertia. Finally, the expectation value of the squared distance converges to a value of the order of the system area L^2 for large times $t - t_0 > 1000\tau$. Arranging P_i randomly, we find an even better agreement with diffusive behavior, $\beta = 1.01$ for $\Pi_K = 0.1$. On the Cayley tree grid such a slow increase of $\langle r_t^2 \rangle$ is absent, it reaches a value of the order of the system area much earlier. This is in agreement with our observation that diffusive power law decay is absent in the transients of tree like grids, Fig. 6 a). In the German transmission grid we find for the node marked by a cross in Fig. 1, that the squared distance $\langle r_t^2 \rangle$ increases more slowly than in the square grid for $\Pi_K = 10$, see Fig. 8 d), in agreement with the insight that the spreading is slowed down in meshed grids. At smaller inertia, corresponding to $\Pi_K = 0.1$, it shows for that node a particular behavior with a delayed spreading followed by a faster spreading of the

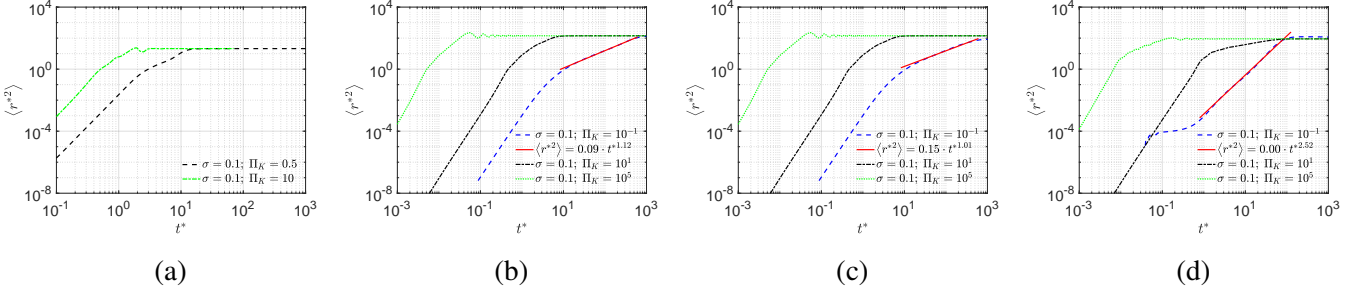


Figure 8: Expectation value of the square of the distance r_i to the origin of power disturbance $\delta P = 0.001P$ as function of time, for the exemplary sets of parameters given in the insets (a) in a Cayley tree grid ($N = 485$), (b) in a square grid ($L = 22$) with periodic arrangement, (c) in a square grid ($L = 22$) with random arrangement, (d) in the German transmission grid with random arrangement of generators and motors.

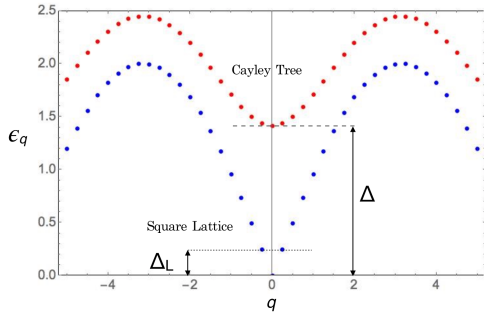


Figure 9: Dispersion ϵ_q as function of discrete wave number q_n for Cayley tree grid (red dots) and square lattice (blue dots). The spectral gap to the first excitation energy is for the Cayley tree grid Δ , (dashed line), while for the square lattice the gap $\Delta_L = \epsilon_{q_1}$ is smaller (dotted line) and decreases with L .

disturbance.

In the next section we present analytical results for the transient behavior for model grids. We show that diffusive spreading of disturbances, is possible in meshed grids like square grids, but that it is absent in tree like grids. This is traced to the presence of a spectral gap in the Laplace operator of these grids.

Spectral Analysis of Disturbances.

Periodic Square Lattice. For a square lattice where the power capacitance K is the same for all transmission lines and generator and consumer power $P_i = \pm P$ is arranged periodically, an analytical solution is obtained with the plain wave Ansatz $\phi_{qi} = c_q e^{i\mathbf{q}\cdot\mathbf{r}_i}$ where \mathbf{q} is the wave vector. The Eigenfrequency ϵ_{q_n} , is obtained as [8],

$$\epsilon_{q_n} = \sqrt{\Pi_K} (1 - \sigma^2/\sigma_c^2)^{1/4} \sqrt{4 - f_{q_n}} \Gamma_0, \quad (6)$$

where $\sigma/\sigma_c = P/(4K)$ and $f_{q_n} = 2(\cos q_{nx}a + \cos q_{ny}a)$. For finite size L , the

wave vectors are quantized, $q_{x,yn} = n_{x,y}\pi/L$, with $n_{x,y} = 0, \pm 1, \dots$. The resulting dispersion of the Eigenfrequency ϵ_q is plotted in Fig. 9 as function of the discrete wave number q_n (blue dots). We observe a gap to the first excitation energy $\epsilon_{q_1} = \Delta_L$ as indicated by the dotted line in Fig. 9, which decreases with size L as

$$\Delta_L = \Pi_K^{1/2} (1 - \sigma^2/\sigma_c^2)^{1/4} \frac{\pi a}{L} \Gamma_0. \quad (7)$$

Inserting $\Lambda_n = \tau^2 \epsilon_{q_n}^2$ into the Fourier expansion Eq. (9), we get the transient behavior of the phase deviation $\alpha(t)$ for all times t . The condition that slow modes with a small relaxation rate appear is, that the spectral gap Δ_L is smaller than the local relaxation rate, Γ_0 . This yields the parametric condition $\Pi_K < \Pi_K^S(L)$, where $\Pi_K^S(L)$ depends on grid size L and ratio σ as

$$\Pi_K^S(L) = (1 - \sigma^2/\sigma_c^2)^{-1/2} \left(\frac{L}{\pi a} \right)^2. \quad (8)$$

This result is plotted in the phase diagram Fig. 6 b) (dashed line) together with numerical results. If the condition $\Pi_K < \Pi_K^S(L)$ is fulfilled, Eigenmodes with small wave number q have purely imaginary Ω_q which results in slow decay of the deviation without oscillations. Summing over all slow modes in the spectral representation of $\alpha_i(t)$, Eq. (9) we find that a perturbation at node j spreads for times $t > \tau$ and distances exceeding the mean free path $l = v_0\tau$. Thus, the initially localized perturbation spreads diffusively with diffusion constant $D = v_0^2\tau/2$, with velocity $v_0 = \sqrt{\Pi_K} \cos \delta_0 a / \tau$, see Suppl. III for the

derivation. Diffusion causes slow power law relaxation of the disturbance at the initial site and an initial increase, followed by a power law decay at other sites. The resulting power law relaxation of the change in transmitted power between nodes k and l is [8]

$$\delta F_{kl}(t) = \pm \delta P A_{kl} \frac{\pi^2 a^2}{\omega_0 D t^2} \exp\left(-\frac{(\mathbf{r}_j - \mathbf{r}_1)^2}{4Dt}\right). \quad (9)$$

Thus, we find analytically that the change in power at the site of the perturbation r_j decays with a power law in time with power 2 in excellent agreement with the numerical results for the periodic square grid, Fig. 5 d). The expectation value of the square of the distance to the perturbation $\langle r_t^2 \rangle$, is for the diffusive propagation at times $t > \tau$, Eq. (17) obtained to be $\langle r_t^2 \rangle = 2Dt$, increasing linearly with time t . After the Thouless time $t_L = L^2/D$ [17], the disturbance reaches the boundary of the grid and is reflected. Then, for times exceeding t_L , the disturbance decays exponentially with rate

$$\Gamma_{min} = (1 - (1 - \tau^2 \Delta^2)^{1/2}) \Gamma_0.$$

For square grids with inhomogenous distribution of power P_i slowly decaying modes appear when $\Pi_K < \Pi_K^s(L)$, with $\Pi_K^s(L)$ given by Eq. (8), where σ_c is the critical value for that distribution of power P_i . Diffusion occurs with an accordingly modified diffusion constant D . We plot $\Pi_K^s(L)$, the dashed line in Fig. 6 c), together with numerical results where we use the numerically obtained value for σ_c .

Cayley Tree Grid. On a Cayley tree grid every inner node is connected to $d = b + 1$ other nodes, as shown in Fig. 1 a) for $b = 3$. For the Cayley tree with branching $b > 1$, the symmetric eigenvectors were found only recently by Mahan in Ref. [18]. Inserting these Eigenvectors into the discrete wave equations Eq. (14) we obtain the Eigenfrequencies

$$\epsilon_q = \sqrt{\Pi_K \sqrt{1 - \frac{\sigma^2}{\sigma_c^2} (b + 1 - 2\sqrt{b} \cos qa)} \Gamma_0}. \quad (10)$$

For $b > 1$, q can not be identified with a wave number since the phase of the Eigenvectors depends nonlinearly on qa . We plot ϵ_q in Fig. 9 for a finite sized tree as function of discrete number q_n . It is remarkable that Eigenfrequencies Eq. (10) have for $b > 1$ a

finite gap Δ , independent on the number of nodes N ,

$$\Delta = \Pi_K^{1/2} (1 - \sigma^2/\sigma_c^2)^{1/4} \sqrt{b + 1 - 2\sqrt{b}} \Gamma_0, \quad (11)$$

as indicated by the dashed line in Fig. 9. The condition that slow modes appear is $\Delta < \Gamma_0$, which yields the parametric condition $\Pi_K < \Pi_K^s$, with

$$\Pi_K^s = (1 - \sigma^2/\sigma_c^2)^{-1/2} (b + 1 - 2\sqrt{b})^{-1}. \quad (12)$$

If that condition is fulfilled, the perturbation decays for large times exponentially with a reduced relaxation rate $\Gamma_{min} = (1 - (1 - \tau^2 \Delta(z, \Pi_K)^2)^{1/2}) \Gamma_0$ which can be much smaller than the local relaxation rate Γ_0 . We plot $\Pi_K^s(\sigma/\sigma_c)$ in Fig. 6 a) as the dashed line. For a tree grid with inhomogenous distribution of power P_i , typically, the slowly decaying modes are expected to appear when $\Pi_K < \Pi_K^s$, with Π_K^s given by Eq. (12), where σ_c is the critical value for that distribution of power P_i .

Discussions. For the german transmission grid the lines have a typical capacity of $K_{ij} = 10$ GW [9]. Assuming that half of the nodes act as generators and the other half as consumers to meet Germany's peak power production of 83 GW [19], we set $|P_i| = 300$ MW. Typical conventional power plants of that rated power have inertia $J = 10^4$ kg m² and damping $\gamma\omega^2 = 0.10P$. This yields $J\omega^3 = 310$ GW, $\Pi_P = 1.03 \cdot 10^5$ and $\Pi_K = 3.44 \cdot 10^6$. Taking the condition $\Pi_K < \Pi_K^s(L)$, with Eq. (12) as an estimate that meshed grids show diffusive behaviour, that condition becomes for currently existing transmission grids, $L > 1856a$. Thus, diffusive propagation is unlikely to occur in present transmission grids even on the European scale. However, as conventional power plants become substituted by renewable energy the inertia in the grid becomes reduced substantially [1]. Thus, the dynamics of transmission grids changes. For small inertia of $J = 0.1$ kg m² and otherwise same parameters, we find $\Pi_P = 1.03$ and $\Pi_K = 34.45$ so that the condition to observe diffusion is $L > 5.87a$ and becomes relevant for transmission grids on the national scale. If no measures are undertaken to substitute the inertia of conventional power plants[20], we conclude that transient dynamics will change drastically, disturbances relaxing slowly and spreading by collective diffusive propagation.

In conclusion, we studied how the relaxation and propagation of disturbances in AC grids is modified when system parameters like the inertia in the grid are changed. To this end we solved the nonlinear swing equations on three different grid topologies numerically and analyzed the results comparing them quantitatively with analytical insights obtained by mapping the swing equations for small perturbations on discrete wave equations. We solved these wave equations by generalized Fourier expansion for the square grid and the Cayley tree grid. Thereby we show that the long time transient behavior is governed by the spectral gap between the stationary state and the lowest Eigenmode of its grid. While the Cayley tree grid has a finite spectral gap, independent on grid size, meshed grids have a small spectral gap which is reduced strongly with increasing grid size, leading to slowed relaxation and collective diffusive propagation of disturbances. Analyzing the numerical results we confirm that, depending on inertia, geographical distribution of power, grid power capacity and topology, the disturbance may either decay exponentially in time with the decay rate of a single node, Γ^0 , or exponentially with a smaller decay rate $\Gamma < \Gamma^0$, or, even more slowly, decaying with a power law in time, resulting in collective diffusive propagation. Such slow decay of disturbances could be prevented by avoiding meshed grids in favour of tree like grids.

Methods

Stationary solution. Before any perturbation is applied, we calculate the stationary state θ_i^0 at every node i in the grid. This is accomplished by first obtaining an analytical solution of Eq. (1) for small phase differences linearizing $\sin(\theta_i^0 - \theta_j^0) \rightarrow \theta_i^0 - \theta_j^0$. Thereby Eq. (1) can be rewritten by introducing the weighted graph Laplacian matrix

$$H_{ij} = -K_{ij} + \delta_{ij} \sum_l K_{il}, \text{ as}$$

$$P_i = \sum_j K_{ij}(\theta_i^0 - \theta_j^0) \Rightarrow \mathbf{P} = H \cdot \boldsymbol{\theta}^0, \quad (13)$$

where \mathbf{P} and $\boldsymbol{\theta}^0$ are vectors, whose i -th component is the power and stationary phase at node i , respectively. H has at least one zero Eigenvalue. Therefore, we need to calculate the pseudo inverse H^+ , yielding $\boldsymbol{\theta}^0 = H^+ \cdot \mathbf{P}$. We use this numerical solution then

as initial condition for a numerical root solver to find the solution of the nonlinear equation, Eq. (1). This way, the numerical accuracy of the stationary solution is maximized which is important, since we use it as initial condition for the swing equation to make sure that we start in stationary conditions.

Numerical Solution of Swing Equations. Having found the stationary phases θ_i^0 as solutions of the stationary state equations Eq. (1), we can insert them into the swing equations Eq. (4). Next, we solve these equations to study the transient behavior when the AC grid is perturbed by a local disturbance as outlined in detail in Suppl. I. We study the transient phase deviation α_i and the phase velocity $\partial_t \alpha_i$, as well as the change in transmitted power between all connected nodes i, j , $\Delta F_{i,j}$. In this article, we are primarily interested to understand the propagation of disturbances which are so small that they do not destabilize the grid.

Analytical Derivation. For small perturbations, corresponding to the parametric condition $\sigma < \sigma^*(\alpha)$, we can analyse the swing equations Eq. (4) by expanding it in the perturbation $\alpha_i - \alpha_j$. This yields the linear wave equations on the grid [8],

$$\tau^2 \partial_t^2 \alpha_i + 2\tau \partial_t \alpha_i + \sum_j t_{ij}(\alpha_i - \alpha_j) = \delta \Pi_i(t),$$

with coupling amplitudes $t_{ij} = \Pi_{Kij} \cos(\theta_i^0 - \theta_j^0)$, depending both on grid topology and on the initial distribution of power P_i through the stationary phases θ_i^0 . These coupling amplitudes t_{ij} form the generalized Laplace operator Λ with $\Lambda_{ij} = -t_{ij}$ and $\Lambda_{ii} = \sum_i t_{ii}$, which is related to the stability matrix in the linear stability analysis [14, 15]. The dimensionless disturbance function is defined by $\delta \Pi_i(t) = J \delta P_i(t) / (\gamma^2 \omega)$. We expand the phase deviation $\alpha_i(t)$ and the disturbance $\delta \Pi_i(t)$ in a generalized Fourier series in terms of the Eigenvectors ϕ_n of Λ , as defined by $\Lambda \phi_n = \Lambda_n \phi_n$, where Λ_n is its Eigenvalue [8, 16, 15, 14], see Suppl. III for a detailed derivation. For a local perturbation at a site j , lasting only a short time interval $\Delta t \ll \tau$ around time t_0 , $\delta \Pi_i(t) = \delta \Pi \delta_{ij} \tau \delta(t - t_0)$, we find

$$\alpha_i(t > t_0) = -\frac{\delta \Pi}{2} \sum_n \phi_{ni} \phi_{nj}^* \frac{1}{\sqrt{1 - \Lambda_n}} \times (e^{-i\Omega_n(t-t_0)} - e^{-i\Omega_n(t-t_0)}), \quad (14)$$

where $\Omega_{n\pm} = -1(1 \pm \sqrt{1 - \Lambda_n})1/\tau$. In order to find the transient dynamics for all times t , it remains to find the Eigenvalues $\Lambda_n \epsilon_n^2 \tau^2$ and Eigenvector components ϕ_{ni} , as can be done numerically for arbitrary grids. For particular grids, analytical solutions can be obtained as we reviewed above and in Suppl. III.

Acknowledgements

We gratefully acknowledge the support of BMBF in the frame of CoNDyNet FK. 03SF0472D.

Supplementary

More information on methods and derivations is provided in the appended supplementary text. For further illustration we also provide three exemplary movies showing the propagation of disturbances in a tree grid, a square grid and the german transmission grid.

Author contributions

Research design and numerics were performed by S.T and M.C., with S.K. supervising the project and performing the analytical calculations. All authors contributed to editing the manuscript.

Competing financial interests

The authors declare no competing financial interests.

References

[1] Ulbig, A., Borsche, T. S. & Andersson, G. Impact of low rotational inertia on power system stability and operation. *IFAC Proceedings Volumes* **14**(3), 7290-7297 (2014).
 [2] Kundur, P. Power System Stability and Control. (Mc Graw Hill, 1994).
 [3] Machowski, J., Bialek, J.W. & Bumby, J.R. Power System Dynamics: Stability and Control. (Wiley, 2008).
 [4] Bergen, A.R. & Hill, D.J. A structure preserving model for power system stability analysis. *IEEE Trans. on Power App. and Syst.* **100**(1), 25-35 (1981).
 [5] Filatrella, G., Nielsen, A.H. & Pedersen, N.F. Analysis of a power grid using a Kuramoto-like model. *Eur Phys. J. B* **61**(4), 485-491 (2008).
 [6] Rohden, M., Sorge, A., Timme, M. & Witthaut, D. Self-organized synchronization in decentralized power grids. *Phys. Rev. Lett.* **109**, 064101 (2012).

[7] Schmietendorf, K., Peinke, J., Friedrich, R. & Kamps, R.O. Self-organized synchronization and voltage stability in networks of synchronous machines. *Eur. Phys. J. Spec. Top.* **223**(12), 2577-2592 (2014).
 [8] Kettemann, S. Delocalization of disturbances and the stability of AC electricity grids. *Phys. Rev. E* **94**, 062311 (2016).
 [9] Matke, C., Medjroubi, W. & Kleinhans, D. *SciGRID - An Open Source Reference Model for the European Transmission Network (v0.2)*, (July 2016).
 [10] Heuck, K., Dettmann, K.D. & Schulz, D. *Elektrische Energieversorgung*, 9th edition. (Springer, 2009).
 [11] Rohden, M. Self-organized Synchronization in Decentralized Power Grids. PhD thesis, (Göttingen, 2014).
 [12] Menck, P.J., Heitzig, J., Kurths, J., & Schellnhuber, H.J. How dead ends undermine power grid stability. *Nature Communications* **5**, 3969 (2014).
 [13] M. Newman, *Networks: An Introduction*. (OUP, Oxford, 2009).
 [14] Coletta, T. & Jacquod, P. Linear stability and the Braess paradox in coupled-oscillator networks and electric power grids. *Phys Rev E* **93**, 032222 (2016).
 [15] Nishikawa, T. & Motter, A.E. Comparative analysis of existing models for power grid synchronization. *New J. Phys.* **17**, 015012 (2015).
 [16] L. A. Torres-Sánchez, G. T. Freitas de Abreu, S. Kettemann, Analysis of the Dynamics and Topology Dependencies of Small Perturbations in Electric Transmission Grids, subm. to IEEE Power Systems, arXiv:1706.10130 (2017).
 [17] Edwards, J.T. & Thouless, D.J. Numerical studies of localization in disordered systems. *J. Phys. C: Solid State Phys.* **5**, 807 (1972).
 [18] Mahan, G.D. Energy bands of the Bethe lattice. *Phys. Rev. B* **63**, 155110 (2001).
 [19] Bayer, E. Report on the German Power System, *Country Profile 057/03-CP-2014/EN*, *Agora Energiewende*. (Berlin, Germany, 2015).
 [20] T. Borsche and F. Dörfler, On Placement of Synthetic Inertia with Explicit Time-Domain Constraints, subm to IEEE Transactions on Power Systems, <https://arxiv.org/abs/1705.03244> (2017).
 [21] E. Kreyszig, *Advanced Engineering Mathematics*, 9th edition., Wiley, New York (2006).

Supplementary

I. Numerical Simulations

We employ a standard differential equation solver, the Runge-Kutta algorithm [21] using the commercial software MATLAB[®]. Since this is a shooting method its convergence is improved considerably by setting the phases to the stationary state solutions before the perturbation. The perturbation is applied at

$t = 0$. Calculated time spans prior and past perturbation were iteratively adjusted to ensure both a stationary state onto which the perturbation is applied and to capture the whole perturbation event until complete decay. Temporal resolution was chosen fine enough to avoid undersampling of the oscillating phases using the phase portraits $\dot{\alpha}_i(\alpha_i)$ as sensors. They would show smooth curves for sufficient resolution or angled curves for too poor resolution. In favour of automatized calculation, time span and resolution were mostly not adapted but rather chosen better than necessary. Concretely, for German and square grid, throughout all values of Π_K , $t \in [-1000\tau, 1000\tau]$ in steps of $10^{-3}\tau$. For the Cayley tree grid, time span and resolution were i) $t \in [-1000\tau, 1000\tau]$ in steps of $10^{-3}\tau$ for $\Pi_K < 10$ and ii) $t \in [-30\tau, 70\tau]$ in steps of $10^{-3}\tau$ for $\Pi_K \geq 10$.

II. Stability

Depending on the magnitude of the disturbance it can destabilize the grid already at smaller values of σ than the critical value σ_c above which there is no stationary solution, $\sigma < \sigma_c$. In order to get a typical upper limit for the size of the perturbation α before it kicks the system out of the stability, let us first disregard the dependence of the phase deviation at node i , α_i , on the perturbation at neighbored sites α_j . This reduces the swing equations Eq. M(5) of the main article to the one of a single damped, driven nonlinear pendulum. For large times $t \gg 0$ it is well known to have two stable solutions: 1. *The stationary solution*: There is a stable fixed point at $\partial_t \alpha_i = 0$, $\alpha_i = n2\pi$, n integer, to which small deviations relax exponentially fast with the local decay rate $\Gamma_0 = 1/\tau$. 2. *The over-swinging pendulum solution*: when the driving force and damping are in balance, the phase velocity oscillates around the value $\delta\omega_i = P_i/(2\gamma\omega)$. There are saddle point solutions at $(\alpha_{si}, \partial_t \alpha = 0)$, where α_{si} is given by

$$\alpha_{si} = -2\arctan \left(\frac{\sum_j \Pi_{Kij} \cos(\theta_i^0 - \theta_j^0)}{\sum_j \Pi_{Kij} \sin(\theta_i^0 - \theta_j^0)} \right). \quad (1)$$

The condition for phase points to lie inside the stability region at node i is then obtained from this local

stability analysis to be approximately given by [8]

$$\alpha_i^2 + \frac{(\tau \partial_t \alpha_i)^2}{(1 + \sqrt{1 - \sum_j \Pi_{Kij} \cos(\theta_i^0 - \theta_j^0 - \alpha_{si})})} \ll \alpha_{si}^2. \quad (2)$$

Thus, we can ensure stability against the perturbation $\alpha(t)$, by making sure that it satisfies the stability condition Eq. (2) for all times t . While that depends on the power distribution P_i and the topology of the grid through the stationary phase angles θ_i^0 , we can get a typical upper limit for the allowed size of the perturbation α by substituting $\sin(\theta_i^0 - \theta_j^0)$ with the typical value of $P_i/(d_i K)$, which we denoted above by σ/σ_c . Substitution into Eq. (1) gives the saddle point value

$\alpha_s = -2\arcsin(\sqrt{1 - \sigma^2/\sigma_c^2})$. Thus, for fixed perturbation amplitude α we find a critical value of σ , above which the disturbance causes instability,

$$\sigma^*(\alpha) = \sigma_c \cos(\alpha/2). \quad (3)$$

We see that the disturbance can destabilize the grid at smaller values $\sigma^*(\alpha) < \sigma_c$. $\sigma^*(\alpha)$ coincides with σ_c only in the limit, when the perturbation amplitude is vanishing, $\sigma^*(\alpha \rightarrow 0) = \sigma_c$.

III. Response to Disturbances

Starting from the linearized wave equation in the presence of a disturbance, obtained by a linear expansion in phase perturbation α_i in the presence of a fluctuation in power δP ,

$$\tau^2 \partial_t^2 \alpha_i + 2\tau \partial_t \alpha_i = \sum_j t_{ij} (\alpha_i - \alpha_j) + \frac{\delta P_i(t)}{J\omega} \tau^2 \quad (1)$$

we define the weighted Laplacian Λ with

$$\Lambda_{ij} = -t_{ij} \quad \text{and} \quad \Lambda_{ii} = \sum_j t_{ij} \quad (2)$$

to obtain

$$\tau^2 \partial_t^2 \vec{\alpha} + 2\tau \partial_t \vec{\alpha} + \Lambda \vec{\alpha} = \frac{\delta P_i(t)}{J\omega} \frac{J^2}{\gamma^2}. \quad (3)$$

Since $\Pi_P = (JP)/(\gamma^2\omega)$, we can introduce

$$\partial \Pi_i = \frac{J \delta P_i(t)}{\gamma^2 \omega}. \quad (4)$$

Thus, we can write the phase deviation $\alpha_i(t)$ as a generalized Fourier series by writing its time dependence as a Fourier integral, and expanding its spatial dependence in terms of the Eigenvectors ϕ_n of the generalized Laplace operator Λ , defined by $\Lambda\phi_n = \Lambda_n\phi_n$, where Λ_n are its Eigenvalues[15, 8, 14]. Thereby we obtain[8, 16]

$$\alpha_i(t) = \int_{-\infty}^{\infty} d\epsilon \sum_n c_{n\epsilon} \phi_{ni} e^{-i\epsilon t}. \quad (5)$$

Expanding the disturbance likewise in a generalized Fourier series we get

$$\delta\Pi_i(t) = \int_{-\infty}^{\infty} d\epsilon \sum_n \eta_{n\epsilon} \phi_{ni} e^{-i\epsilon t}. \quad (6)$$

Now, we can insert both expansions into Eq. M(9) and find, requiring that the equation is fulfilled for each term of the Fourier series,

$$(-\tau^2\epsilon^2 - i2\tau\epsilon + \Lambda_n) c_{n\epsilon} = \eta_{n\epsilon}. \quad (7)$$

For given disturbance, the Fourier component of the phase deviation $c_{n\epsilon}$ is thus given in response to the one of the disturbance $\eta_{n\epsilon}$. Inserting that expression for $c_{n\epsilon}$ back into the Fourier series we get

$$\alpha_i(t) = \int_{-\infty}^{\infty} d\epsilon \sum_n (-\tau^2\epsilon^2 - i2\tau\epsilon + \Lambda_n)^{-1} \eta_{n\epsilon} \phi_{ni} e^{-i\epsilon t}. \quad (8)$$

The integral over the angular frequency ϵ can be performed by means of the residuum theorem, noting that there are two poles in the lower complex plane, $\epsilon_{n\pm} = -i(1 \pm \sqrt{1 - \Lambda_n})/\tau$. We note that the coefficients $\eta_{n\epsilon}$ are complex and depend on ϵ . If the disturbance sets in at time t_0 , $\eta_{n\epsilon}$ has a phase factor $\exp(i\epsilon t_0)$. Thus, for $t > t_0$, the integrand is convergent in the lower complex plane, so that we can close the integration contour there, and obtain

$$\alpha_i(t > t_0) = -\frac{\pi}{\tau} \sum_n \phi_{ni} \frac{1}{\sqrt{1 - \Lambda_n}} \times (\eta_{n\epsilon_{n+}} e^{-i\epsilon_{n+}t} - \eta_{n\epsilon_{n-}} e^{-i\epsilon_{n-}t}).$$

For $t < t_0$ the integrand is convergent in the upper complex plane, where there are no poles, so that the residuum is vanishing and we find $\alpha_i(t < t_0) = 0$. Eq. (9) is valid in linear order for any perturbation

$\delta\Pi_i(t)$ and any electricity grid, inserting the Eigenvalues Λ_n and Eigenvector components ϕ_{ni} of the respective Laplacian.

For a local perturbation at a site j lasting only a short time interval $\Delta t \ll \tau$ around time t_0 , we can choose the perturbation as $\delta\Pi_i(t) = \delta\Pi\delta_{ij}\tau\delta(t - t_0)$. Fourier transformation gives $\eta_{n\epsilon} = \frac{1}{2\pi}\delta\Pi\tau\phi_{nj}^*e^{i\epsilon t_0}$. Insertion into Eq. (9) gives then

$$\alpha_i(t > t_0) = -\frac{\delta\Pi}{2} \sum_n \phi_{ni}\phi_{nj}^* \frac{1}{\sqrt{1 - \Lambda_n}} \times (e^{-i\epsilon_{n+}(t-t_0)} - e^{-i\epsilon_{n-}(t-t_0)}). \quad (10)$$

Thus, it remains to find the Eigenvalues Λ_n and Eigenvector components ϕ_{ni} .

Square Grid. For a square grid with transmission line length a and power capacitance K and periodically arranged generator and consumer power $P_i = \pm P$, the Eigenvectors are plain waves with $\phi_{qni} = c_{qn} e^{i\mathbf{q}\mathbf{n}\mathbf{r}_i}$, where \mathbf{q}_n is the wave vector which takes on a grid of finite size L discrete values, $\mathbf{q}_n = (n_x, n_y)\pi/L$, where $n_x, n_y \in \{-L/(2a), \dots, +L/(2a)\}$. The Eigenvalues of the Laplacian Λ are given by $\Lambda_n = \tau^2\epsilon_{qn}^2$, where the Eigenfrequency ϵ_q of the linear wave equation is[8],

$$\epsilon_q = \sqrt{\Pi_K}(1 - \sigma^2/\sigma_c^2)^{1/4} \sqrt{4 - f_q}\Gamma_0, \quad (11)$$

where $\sigma/\sigma_c = P/(4K)$ and $f_q = 2(\cos q_x a + \cos q_y a)$. Insertion in Eq. (10) thus yields the phase perturbation in response to a change of the power at time t_0 at site j , $\delta\Pi_i(t)$ as

$$\alpha_i(t > t_0) = \delta\Pi \frac{1}{N} e^{-(t-t_0)/\tau} \sum_{n_x, n_y} e^{i\mathbf{q}_n(\mathbf{r}_i - \mathbf{r}_j)} \times \frac{\sinh\left(\frac{t-t_0}{\tau} \sqrt{1 - \Lambda_n}\right)}{\sqrt{1 - \Lambda_n}}. \quad (12)$$

Thus, inserting all Eigenvalues $\Lambda_n = \tau^2\epsilon_{qn}^2$ with Eq. (11) we get the transient behavior of the phase deviation for all times $t > t_0$. For large momenta q , the ballistic limit, the relaxation is fast with the local rate Γ_0 and there is a real frequency with linear dispersion, $\Omega_q|_{q \ll 0} \approx -i\Gamma_0 + v_0 q$ with velocity $v_0 = \sqrt{\Pi_K} \cos \delta_0 a/\tau$. At large time $t \gg \tau$ all such modes with Eigenvalues $\Lambda_n > 1$ have decayed.

Depending on the system parameters there can exist slow modes with $\Lambda_n < 1$, which decay with smaller rate $\Gamma_{n-} = \Gamma_0(1 - (1 - \Lambda_n)^{1/2})$. If this condition is fulfilled, Eigenmodes with small wave number q appear whose Eigenfrequency is purely imaginary, $\Omega_q = -i\Pi_K \cos \delta_0 a^2 \mathbf{q}^2$, which decay slowly without oscillations. Then, summing over all modes in the spectral representation of $\alpha_i(t)$, we find that an initially localized perturbation at node l spreads for times $t > \tau$ and distances exceeding the mean free path $l = v_0\tau$, $|r_i - r_l| > l$, using the continuum limit

$$\sum_{\vec{q}} \rightarrow \frac{1}{\left(\frac{2\pi}{L}\right)^2} \int d\vec{q}, \quad (13)$$

according to

$$\alpha_i(t) = \delta\Pi \frac{1}{N} \frac{L^2}{4\pi^2} \int_{-\pi/a}^{+\pi/a} dk_x \int_{-\pi/a}^{+\pi/a} dk_y \quad (14)$$

$$\times e^{i(k_x \hat{e}_{ijx} a + k_y \hat{e}_{ijy} a)} e^{-(t-t_0)D(k_x^2 + k_y^2)},$$

yielding

$$\alpha_i(t) = \frac{\alpha_0 a^2}{4\pi D_0 t} \exp\left(-\frac{(\mathbf{r}_i - \mathbf{r}_l)^2}{4D_0 t}\right). \quad (15)$$

Thus, the initially localized perturbation spreads diffusively with diffusion constant

$$D = v_0^2 \tau / 2 = \Pi_K (1 - \sigma^2 / \sigma_c^2)^{1/2} a^2 / (2\tau). \quad (16)$$

Diffusion causes very slow power law relaxation of the disturbance at the initial site, and an initial increase, followed by a slow power law decay at other sites. The resulting power law relaxation of the change in transmitted power between nodes k and l is then obtained to be [8]

$$\delta F_{kl}(t) = \pm \delta P A_{kl} \frac{\pi^2 a^2}{\omega_0 D t^2} \exp\left(-\frac{(\mathbf{r}_i - \mathbf{r}_l)^2}{4Dt}\right). \quad (17)$$